

This work was written as part of one of the author's official duties as an Employee of the United States Government and is therefore a work of the United States Government. In accordance with 17 U.S.C. 105, no copyright protection is available for such works under U.S. Law. Access to this work was provided by the University of Maryland, Baltimore County (UMBC) ScholarWorks@UMBC digital repository on the Maryland Shared Open Access (MD-SOAR) platform.

Please provide feedback

Please support the ScholarWorks@UMBC repository by emailing [scholarworks-group@umbc.edu](mailto:scholarworks-group@umbc.edu) and telling us what having access to this work means to you and why it's important to you. Thank you.



# High-Frequency Noise Peaks in Mo/Au Superconducting Transition-Edge Sensor Microcalorimeters

N. A. Wakeham<sup>1,2</sup>  · J. S. Adams<sup>1,2</sup> · S. R. Bandler<sup>1</sup> · S. Beaumont<sup>1,2</sup> · M. P. Chang<sup>1,3</sup> · J. A. Chervenak<sup>1</sup> · A. M. Datesman<sup>1,3</sup> · M. E. Eckart<sup>4</sup> · F. M. Finkbeiner<sup>1,5</sup> · J. Y. Ha<sup>1,6</sup> · R. Hummatov<sup>1,2</sup> · R. L. Kelley<sup>1</sup> · C. A. Kilbourne<sup>1</sup> · A. R. Miniussi<sup>1,2</sup> · F. S. Porter<sup>1</sup> · J. E. Sadleir<sup>1</sup> · K. Sakai<sup>1,2</sup> · S. J. Smith<sup>1,2</sup> · E. J. Wassell<sup>1,3</sup>

Received: 17 July 2019 / Accepted: 26 December 2019  
© Springer Science+Business Media, LLC, part of Springer Nature 2020

## Abstract

The measured noise in Mo/Au transition-edge sensor (TES) microcalorimeters produced at NASA has recently been shown to be well described by a two-body electrothermal model with a finite thermal conductance between the X-ray absorber and the TES. In this article, we present observations of a high-frequency peak in the measured current noise in some of these devices. The peak is associated with an oscillatory component of the TES response that is not predicted in a single-body model but can be qualitatively described by the two-body model.

**Keywords** Transition-edge sensor · Microcalorimeter · Multi-body

## 1 Introduction

Superconducting transition-edge sensor (TES) microcalorimeters produced at NASA's Goddard Space Flight Center are the baselined technology for the X-ray Integral Field Unit instrument on the Advanced Telescope for High-ENERgy Astrophysics (ATHENA) [1]. These microcalorimeters must be capable of simultaneously achieving all the challenging performance requirements of the instrument, such as

---

✉ N. A. Wakeham  
nicholas.a.wakeham@nasa.gov

<sup>1</sup> NASA Goddard Space Flight Center (GSFC), Greenbelt, MD 20771, USA

<sup>2</sup> CRESST II – University of Maryland, Baltimore County, MD 21250, USA

<sup>3</sup> Science Systems and Applications, Inc. (SSAI), 10210 Greenbelt Rd, Lanham, MD 20706, USA

<sup>4</sup> Lawrence Livermore National Laboratory (LLNL), Livermore, CA 94550, USA

<sup>5</sup> Sigma Space Corp., 4600 Forbes Blvd., Lanham, MD 20706, USA

<sup>6</sup> SB Microsystems, 806 Cromwell Park Dr, Glen Burnie, MD 21061, USA

energy resolution, energy range and X-ray count rate. In order to do this, it is important to have extremely close control and knowledge of all the intrinsic properties of these devices.

In the simplest model of a TES microcalorimeter, the noise sources can be calculated by treating the TES as a normal resistor, and the thermal model of the device as a single thermal body connected to a heat bath by a single thermal conductance term [2–4]. A long standing problem with superconducting TES devices has been the measurement of noise in excess of the predictions from this simple model [4–6]. Many experimental and theoretical works have presented explanations for this so-called excess noise by adding additional complexity to the treatment of either the TES electrical behavior or the thermal model of the microcalorimeter [7–10]. Recent work by our group presented evidence that, despite the excellent energy resolution they can achieve, a significant source of noise in our Mo/Au TES microcalorimeters is from internal thermal fluctuations between the Bi/Au X-ray absorber and the TES [11]. These fluctuations produce significant noise because of a finite thermal conductance between these two regions of the device. The magnitude and dependencies of that finite internal thermal conductance were shown to be consistent with it originating from the thermal conductance of the TES bilayer itself.

In this article, we show experimental observations of a high-frequency peak in the measured current noise of some of our TES devices over a small range of the bath temperature and TES-biased resistance. The two-body model described above is able to qualitatively explain this behavior as arising from an oscillatory component in the solution of the two-body electro-thermal equations. This is strong evidence that a multi-body description of these Mo/Au TES microcalorimeters should be included in any discussion of the noise behavior. This knowledge will enable more accurate modeling of the microcalorimeter performance, and in the future may give routes to further improvements in the TES design.

## 2 Methods

The TES microcalorimeters discussed in this article consist of a TES made of a Mo/Au bilayer (thickness 35/172 nm) placed at the center of silicon nitride membrane that extends to a Si frame that is well heat sunk and forms the thermal bath. The sheet resistance of the bilayer was  $22 \text{ m}\Omega/\square$ . The TES is connected to a  $240 \mu\text{m}$  square Bi/Au absorber by two Au pillar-shaped stems that are  $\sim 4 \mu\text{m}$  tall and  $10 \mu\text{m}$  in diameter. Electrical connection to the TES bilayer is made with Nb leads. Additional details of the device design and fabrication are discussed elsewhere [4, 6]. The measurements presented here were taken using TES's with a range of sizes and aspect ratios. The TES width and length vary from 70–130  $\mu\text{m}$ . A schematic diagram of the TES is shown in Fig. 1.

In order to model the microcalorimeter behavior, it is necessary to measure many different intrinsic properties. The TES is placed in the circuit shown in Fig. 1. The thermal conductance  $G_{\text{bath}}$  was calculated through fitting of the Joule power when the TES was biased to a resistance  $R$  that is 50% of the normal state resistance  $R_N$  at different bath temperatures.  $R_N$  in the devices discussed here ranges from 10–30  $\text{m}\Omega$

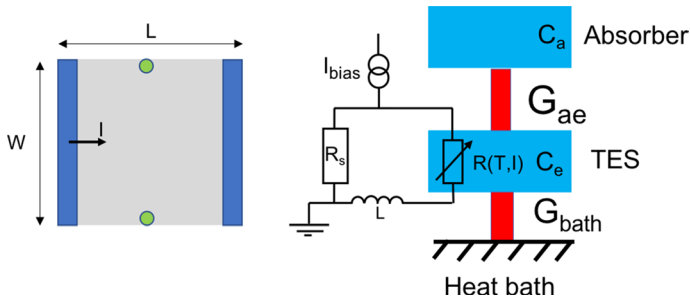


**Fig. 1** Left—Schematic diagram of TES device viewed from above with absorbers removed for clarity. Mo/Au bilayer is shown in gray, electrical connection with Nb leads shown in blue. Green circles indicate Au pillar attachments to a Bi/Au absorber. Arrow shows direction of current  $I$ .  $W$  and  $L$  indicate the width and length of the TES, respectively. Right—Schematic diagram of two-body thermal model of microcalorimeter with electrical circuit also shown.  $C_a$  and  $C_e$  are the heat capacity of the absorber and TES, respectively.  $G_{ae}$  and  $G_{bath}$  are the thermal conductance between the two bodies and from the TES to the bath, respectively. Reproduced from [11] (Color figure online)

and, when  $T_{bath} = 55$  mK, a typical Joule power is  $\sim 1.8$  pW when biased to 50% of  $R_N$ .  $G_{bath} \sim 90$  pW/K at the superconducting transition temperature  $T_c$  where  $T_c$  is typically  $\sim 85$  mK. The total heat capacity of the TES was calculated from measurements of the decay time of an X-ray pulse measured at a bath temperature  $T_{bath}$  close to  $T_c$ , where electro-thermal feedback is negligible. TES noise spectra were calculated from the Fourier transform of the measured current through the TES. This current was measured using a superconducting quantum interference device (SQUID) with a 250 kHz Bessel low-pass filter of 12 dB/Oct. Any residual magnetic field in the experimental apparatus normal to the plane of the TES was nulled by the application of an additional field from a wire coil. Complex impedance of the TES circuit was measured in the range of 10 Hz–5 kHz with the TES biased at different known fractions of  $R_N$ . Complex impedance measurements with zero DC bias current can be used to calculate the inductance of the circuit, which is typically  $\sim 85$  nH. Further details of these measurement techniques are shown elsewhere [2, 4, 11–13].

### 3 Theory

In the single-body model of a microcalorimeter, the system is described by two coupled differential equations [12]. There are two eigenvalues to these equations that dictate the ‘rise-time’ and ‘fall-time’ response of the TES to a delta-function impulse of heat into the system. In certain limits, such as large inductance  $L$ , these two time constants become complex and are complex conjugates of one another, indicating an oscillatory response to the heat impulse. The system is then described as underdamped. In extreme cases, this can lead to a peak in the measured noise spectrum. When this occurs in our devices, it is often well described by the single-body model and the peak frequency is typically of order 1–10 kHz.

The differential equations that describe the response of the linearized two-body model shown in Fig. 1 are given by [9, 11, 14],

$$\begin{aligned}
& \frac{d}{dt} \begin{pmatrix} \Delta I \\ \Delta T_e \\ \Delta T_a \end{pmatrix} \\
&= \begin{bmatrix} -(1/L)[R(1 + \beta) + R_s] & -(\alpha IR/LT_e) & 0 \\ (2 + \beta)(IR/C_e) & -[G_{\text{bath}} + G_{\text{ae}}^{\text{tes}} - (\alpha I^2 R/T)]/C_e & G_{\text{ae}}^a/C_e \\ 0 & G_{\text{ae}}^{\text{tes}}/C_a & -G_{\text{ae}}^a/C_a \end{bmatrix} \begin{pmatrix} \Delta I \\ \Delta T_e \\ \Delta T_a \end{pmatrix} \\
&+ \begin{pmatrix} e_{\text{tes}}(t)/L + e_{\text{shunt}}(t)/L \\ p_{\text{bath}}(t) + p_{\text{ae}}(t) - Ie_{\text{tes}}(t) \\ W(t) - p_{\text{ae}}(t) \end{pmatrix}
\end{aligned} \tag{1}$$

where  $I$  is the current through the TES,  $T_e$  is the temperature of the TES, and  $T_a$  is the temperature of the absorber. Superscripts to the  $G$  terms indicate the temperature of the body at which the thermal conductance is used. The transition parameters of the TES are defined in the usual way by,  $\alpha = \left. \frac{T}{R} \frac{\partial R}{\partial T} \right|_I$  and  $\beta = \left. \frac{I}{R} \frac{\partial R}{\partial I} \right|_T$  [2].  $W(t)$  is a power input into the absorber that is taken as a delta function of time at  $t = 0$ . The total energy input is arbitrary but is typically assumed to be 6 keV.  $e_{\text{tes}}$  and  $e_{\text{shunt}}$  are the Johnson voltage noise terms from the TES and shunt, respectively.  $p_{\text{bath}}$  and  $p_{\text{ae}}$  are the thermodynamic noise from the TES to the bath and the absorber to the TES, respectively. These four noise terms are defined in frequency space, as described in [11]. These differential equations now have three eigenvalues corresponding to the three time constants of this more complex system. As in the single-body model, there is an oscillatory component of the response of the system to a perturbation if two of these eigenvalues become complex and are complex conjugates of one another [15]. When this oscillatory component is large enough, it will give rise to a peak in the noise spectrum.

## 4 Results

The current noise was measured in a TES of width 80  $\mu\text{m}$  and length 120  $\mu\text{m}$  at different bias points within the resistive transition, with  $T_{\text{bath}} = 55$  mK. This noise is shown in Fig. 2 as a function of frequency. For the curve at  $R/R_N = 2.5\%$  at around 100kHz, a large sharp peak is evident in the measured noise. This feature is more rounded at  $R/R_N = 5\%$ , before being suppressed at  $R/R_N = 7.5\%$  and above. Note that our devices are typically operated above  $R/R_N = 10\%$ , and therefore away from these noise peaks.

To try to understand the noise peaks observed in our devices, we have fit the measured noise spectrum shown in Fig. 3 using the two-body model shown in Fig. 1 and several simplifying assumptions. The measured complex impedance (not shown) was fitted simultaneously using this model to extract  $\alpha$  and  $\beta$  of the transition. Note that, as shown in [11], over the measured frequency range the other parameters of the model are not well constrained in the complex impedance fits alone. The heat capacity of the TES  $C_e$  was assumed to be the BCS theoretical value for the volume

**Fig. 2** Current noise as a function of frequency for a TES with width  $80\ \mu\text{m}$  and length  $120\ \mu\text{m}$  at various bias points within the resistive transition with bath temperature  $T_{\text{bath}} = 55\ \text{mK}$  (Color figure online)

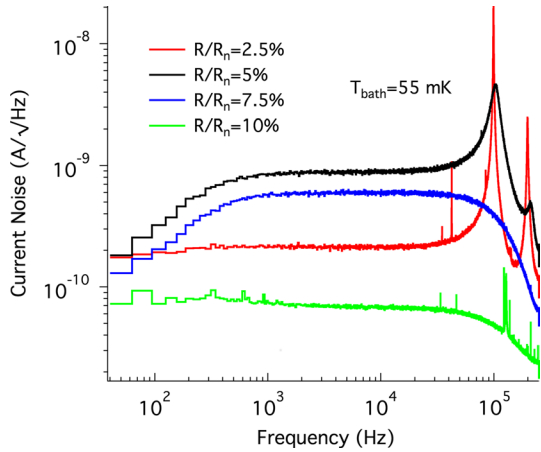
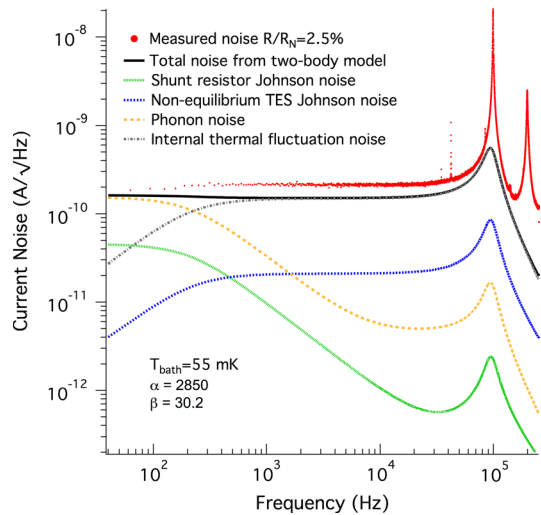


**Fig. 3** Current noise as a function of frequency for a TES with width  $80\ \mu\text{m}$  and length  $120\ \mu\text{m}$  biased at  $R/R_N = 2.5\%$  and  $T_{\text{bath}} = 55\ \text{mK}$  (red dots) and a fit of the total noise calculated in the two-body model shown in Fig. 1 (black line). The different components of the total calculated noise are shown in dashed lines. Detailed descriptions of these noise terms are shown elsewhere [11] (Color figure online)



of material in this particular pixel, at the maximum of the superconducting jump at  $T_c$ , plus a small contribution of  $0.01\ \text{pJ/K}$  from the silicon nitride membrane.  $G_{\text{bath}}$  and the total heat capacity were taken as the measured values for the device. The absorber heat capacity  $C_a$  was assumed to be the difference between the measured heat capacity and  $C_e$ . These assumptions constrain the problem to fitting a single free parameter, the internal thermal conductance between the absorber and the TES  $G_{\text{ae}}$ . These assumptions are described more fully in previous work and were shown there to give reasonable fits to the measured noise [11]. Note that in those previous measurements there were no well defined peaks in the noise spectra.

Figure 3 shows the measured noise spectrum from Fig. 2 at  $R/R_N = 2.5\%$ , along with a fit to the noise using the two-body model described above. This model predicts the peak in the noise spectrum at around  $100\ \text{kHz}$ . The fitted  $G_{\text{ae}}$  in this

example is 50 nW/K. This is the same order of magnitude as found in previous devices with different geometries and  $R_N$ , which did not show this peak in the noise [11]. 50 nW/K is also the same magnitude as the sheet thermal conductance of the TES bilayer calculated using the Wiedemann–Franz law and the measured electrical sheet resistance ( $22.4 \text{ m}\Omega/\square$ ). Therefore, the presence of a peak in the noise spectrum in the case discussed here is a consequence of the particular values of  $L$ ,  $\alpha$  and  $\beta$  and not a result of atypical values in the thermal model.

Although the two-body model is able to qualitatively capture the peak in the measured noise in our device, it is clear that it slightly underestimates the magnitude of the noise at all frequencies, and the measured peak is significantly sharper than the model predicts. Better agreement cannot be found within the constrained model we discuss here. Calculations have shown that in certain limits the two-body model is very sensitive to the exact parameters of the model, for example of  $C_a$  and  $C_e$  [13, 15]. This makes modeling such a dramatic feature extremely challenging but may mean that by relaxing our assumptions of these parameters one could find a better fit to the data. Unfortunately, if many parameters of the model are allowed to be free then degeneracy of the parameters means that the fits to the available data are too unconstrained to be meaningful. With more measurements of these dramatic features over a wide range of parameter space, it may be possible in the future to further refine our model parameters and obtained better fits to the data. Here, we merely demonstrate that this kind of noise peak can be naturally explained, albeit qualitatively, as a consequence of underdamping in a two-body system. Note that in the presence of this underdamped responsivity all noise sources show a peak at the oscillation frequency. Thus, while the two-body thermal model may be an accurate description of the frequency dependence of the measured noise, the discrepancy between the magnitude of the modeled and measured noise may be the result of an additional noise source not considered here. Evidence of such noise sources in some of these devices have been discussed elsewhere [11, 16].

One way to further constrain the two-body model would be to fit the pulse response of the device to the absorption of a photon. Because of nonlinearity of the transition shape, this pulse would need to be sufficiently small to stay within the small signal limit described by our linearized model. To date, we have only measured pulses from 6 keV X-rays, which are well beyond the small signal limit. Measurement of low energy photons with these devices could be an interesting area of future study.

One other interesting feature in the measured noise shown in Fig. 2 is the additional noise peaks observed at integer multiples of the frequency of the main peak. These additional noise peaks cannot be described within our linearized two-body model and likely arise from nonlinearity in the system. This nonlinearity could be from the electrical circuit or the TES response to changes in current and temperature. We have observed that these higher order peaks are not altered by changes to the external electronics, such as SQUID feedback parameters and readout electronics. Therefore, it appears this is intrinsic to the electro-thermal system of the TES.

The measured current noise in a TES of width  $130 \mu\text{m}$  and length  $70 \mu\text{m}$  is shown in Fig. 4 as a function of frequency at 5%  $R_n$  for different values of  $T_{\text{bath}}$ . This figure shows the absence of the noise peak at low bath temperature, in

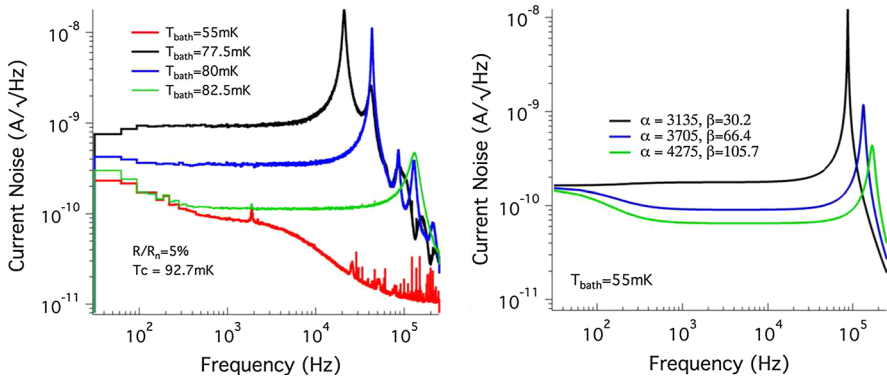


**Fig. 4** *Left* Current noise as a function of frequency for various values of  $T_{\text{bath}}$  for a TES with width  $130\ \mu\text{m}$  and length  $70\ \mu\text{m}$  biased at  $R/R_N = 5\%$ . *Right*—Current noise spectrum predicted by two-body model. All parameters in the model are kept fixed except for  $\alpha$  and  $\beta$  is different in each line, as indicated (Color figure online)

contrast to Fig. 2. The peak is then observed at  $T_{\text{bath}} = 77.5\ \text{mK}$  and above, with the peak frequency increasing with increasing bath temperature, but the magnitude of the noise decreasing. This is likely a consequence of the changing transition shape and physical parameters of this TES with  $T_{\text{bath}}$ , but more quantitative analysis will require highly detailed modeling of the system. The right of Fig. 4 shows the effect on the predicted noise in the two-body model of changing  $\alpha$  and  $\beta$  values. Increasing  $\alpha$  and  $\beta$  can reduce the magnitude of the noise and increase the peak frequency. These data and models demonstrate the sensitivity of the noise peak to the various parameters of the system.

## 5 Conclusion

In conclusion, we have observed high-frequency peaks in the measured current noise of Mo/Au TES microcalorimeters. These dramatic features in the noise are an excellent test of our understanding of the relevant electro-thermal modeling of our devices. We have shown that they are qualitatively consistent with the two-body electro-thermal model presented for these devices previously [11]. This is further evidence that a multi-body description should be considered when describing the behavior of these devices. However, quantitative understanding of these features will require more precise knowledge of the device parameters and a more precise electro-thermal model.

**Acknowledgements** The authors wish to thank NASA's Astrophysics Division for their generous support of this work. This work was performed in part under the auspices of the U.S. Department of Energy by Lawrence Livermore National Laboratory under Contract DE-AC52-07NA27344.

## References

1. D. Barret, T.L. Trong, J.-W. den Herder, L. Piro, X. Barcons, J. Huovelin, R. Kelley, J.M. Mas-Hesse, K. Mitsuda, S. Paltani, G. Rauw, A. Rożanska, J. Wilms, M. Barbera, E. Bozzo, M.T. Ceballos, I. Charles, A. De-courchelle, R. den Hartog, J.-M. Duval, F. Fiore, F. Gatti, A. Goldwurm, B. Jackson, P. Jonker, C. Kilbourne, C. Macculi, M. Mendez, S. Molendi, P. Orleanski, F. Pajot, E. Pointecouteau, F. Porter, G.W. Pratt, D. Prêle, L. Ravera, E. Renotte, J. Schaye, K. Shinozaki, L. Valenziano, J. Vink, N. Webb, N. Yamasaki, F. Delcelier-Douchin, M.L. Du, J.-M. Mes-nager, A. Pradines, G. Branduardi-Raymont, M. Dadina, A. Finoguenov, Y. Fukazawa, A. Janiuk, J. Miller, Y. Nazé, F. Nicastro, S. Sciortino, J.M. Torrejon, H. Geoffray, I. Hernandez, L. Luno, P. Peille, J. André, C. Daniel, C. Etcheverry, E. Gloaguen, J. Hassin, G. Hervet, I. Maussang, J. Moueza, A. Paillet, B. Vella, G.C. Garrido, J.-C. Damery, C. Panem, J. Panh, S. Bandler, J.-M. Biffi, K. Boyce, A. Clénet, M. DiPirro, P. Jamotton, S. Lotti, D. Schwander, S. Smith, B.-J. van Leeuwen, H. van Weers, T. Brand, B. Cobo, T. Dausser, J. de Plaa, E. Cucchetti, *Proc. SPIE*, **9905**, 9905 (2016). <https://doi.org/10.1117/12.2232432>
2. M.A. Lindeman, S. Bandler, R.P. Brekosky, J.A. Chervenak, E. Figueroa-Feliciano, F.M. Finkbeiner, M.J. Li, C.A. Kilbourne, *Rev. Sci. Instrum.* **75**, 1283 (2004). <https://doi.org/10.1063/1.1711144>
3. K. Irwin, *Nucl. Instrum. Methods Phys. Res. Sect. A* **559**, 718 (2006). <https://doi.org/10.1016/j.nima.2005.12.115>
4. S.J. Smith, J.S. Adams, C.N. Bailey, S.R. Bandler, S.E. Busch, J.A. Chervenak, M.E. Eckart, F.M. Finkbeiner, C.A. Kilbourne, R.L. Kelley, S.-J. Lee, J.-P. Porst, F.S. Porter, J.E. Sadleir, *J. Appl. Phys.* **114**, 074513 (2013). <https://doi.org/10.1063/1.4818917>
5. J. Ullom, W. Doriese, G. Hilton, J. Beall, S. Deiker, K. Irwin, C. Reintsema, L. Vale, Y. Xu, *Nucl. Instrum. Methods Phys. Res. Sect. A* **520**, 333 (2004). <https://doi.org/10.1016/j.nima.2003.11.260>
6. N.A. Wakeham, J.S. Adams, S.R. Bandler, J.A. Chervenak, A.M. Datesman, M.E. Eckart, F.M. Finkbeiner, R.L. Kelley, C.A. Kilbourne, A.R. Miniussi, F.S. Porter, J.E. Sadleir, K. Sakai, S.J. Smith, E.J. Wassell, W. Yoon, *J. Low Temp. Phys.* **193**, 231 (2018). <https://doi.org/10.1007/s10909-018-1898-z>
7. C.M. Knoedler, *J. Appl. Phys.* **54**, 2773 (1983). <https://doi.org/10.1063/1.332306>
8. M. Galeazzi, I.E.E.E. *Trans. Appl. Supercond.* **21**, 267 (2011). <https://doi.org/10.1109/TASC.2010.2091243>
9. M. Lindeman, *Microcalorimetry and the Transition-Edge Sensor*, Ph.D. thesis, University of California at Davis (2000)
10. H. Hoevers, A. Bento, M. Bruijn, L. Gottardi, M. Korevaar, W. Mels, P. de Korte, *Nucl. Instrum. Methods Phys. Res. Sect. A* **444**, 192 (2000). [https://doi.org/10.1016/S0168-9002\(99\)01356-X](https://doi.org/10.1016/S0168-9002(99)01356-X)
11. N.A. Wakeham, J.S. Adams, S.R. Bandler, S. Beaumont, J.A. Chervenak, A.M. Datesman, M.E. Eckart, F.M. Finkbeiner, R. Hummatov, R.L. Kelley, C.A. Kilbourne, A.R. Miniussi, F.S. Porter, J.E. Sadleir, K. Sakai, S.J. Smith, E.J. Wassell, *J. Appl. Phys.* **125**, 164503 (2019). <https://doi.org/10.1063/1.5086045>
12. K.D. Irwin, G.C. Hilton, *Cryogenic Particle Detection*, vol. 99 (Springer, Berlin, 2005)
13. I.J. Maasilta, *AIP Adv.* **2**, 042110 (2012). <https://doi.org/10.1063/1.4759111>
14. E. Figueroa-Feliciano, *J. Appl. Phys.* **99**, 114513 (2006). <https://doi.org/10.1063/1.2191449>
15. D.A. Bennett, R.D. Horansky, A.S. Hoover, N.J. Hoteling, M.W. Rabin, D.R. Schmidt, D.S. Swetz, L.R. Vale, J.N. Ullom, *Appl. Phys. Lett.* **97**, 102504 (2010). <https://doi.org/10.1063/1.3486477>
16. A. Wessels, K. Morgan, D.T. Becker, Jo.D. Gard, G.C. Hilton, J.A.B. Mates, C.D. Reintsema, D.R. Schmidt, D.S. Swetz, J.N. Ullom, L.R. Vale, D.A. Bennett, [arXiv:1907.11343](https://arxiv.org/abs/1907.11343) [cond-mat.supr-con]

**Publisher's Note** Springer Nature remains neutral with regard to jurisdictional claims in published maps and institutional affiliations.